

## Supporting Information

### *Experimental Sections*

**Preparation of MXene nanosheets:** 1 g of lithium fluoride powder was dissolved in 10 mL of concentrated hydrochloric acid (12 M). Subsequently, 1 g of  $\text{Ti}_3\text{AlC}_2$  powder was added gradually to the above solution in a course of 10 min to avoid overheat and then the mixture was kept in a water bath of 35 °C for 24 h under magnetic stirring. The resulting mixture was washed with deionized water and centrifuged at 3500 rpm several times until the pH was close to 7. After gentle sonication for 1 h, the ultrathin MXene nanosheets were obtained from the supernatant after being centrifuged at 3500 rpm. The final product was collected via lyophilization.<sup>1</sup>

**Preparation of  $\text{Co}_3\text{O}_4$  QDs:** 160 mg of cobalt(II) acetate was added to 7 mL of benzyl alcohol and stirred at 25 °C for 2 h. 7 mL of ammonium hydroxide (25 wt%) was instilled into a balloon flask under magnetic stirring. Then the flask was transferred to an oil bath of 165 °C and kept for 2 h under magnetic stirring. The resulting black suspension was washed by centrifugation with diethyl ether and ethanol. The black precipitate was collected and dried in vacuum at 80 °C overnight.<sup>2</sup>

**Preparation of  $\text{Co}_3\text{O}_4$  QDs/MXene hybrids:** The MXene nanosheets and  $\text{Co}_3\text{O}_4$  QDs were dispersed in THF separately at a concentration of 1 mg mL<sup>-1</sup>. Then, the two dispersions were mixed at different mass ratios ( $\text{Co}_3\text{O}_4$  : MXene = 1:1, 2:1 and 3:1). The mixed dispersions were sonicated gently for 10 h under argon atmosphere protection. At last, the products were collected through vacuum filtration and dried in vacuum at 50 °C overnight.

**Electrochemical tests:** 2025 coin-type half cells were assembled to evaluate the electrochemical performance. The working electrode slurry was fabricated by mixing 80 wt% active material (MXene,  $\text{Co}_3\text{O}_4$  QDs and  $\text{Co}_3\text{O}_4$  QDs/MXene), 10 wt% conductive agent (acetylene black) and 10 wt% binder (5 wt% poly(vinylidene fluoride) dissolved in *N*-methyl-2-pyrrolidone) at room temperature. Then the resulting slurry was coated on copper foils and dried in vacuum at 120 °C overnight. Half cells were assembled in an argon-filled glove box using lithium foils as the counter electrodes. The electrolyte consisted of 1 M  $\text{LiPF}_6$  dissolved in ethylene carbonate/diethyl carbonate (volume ratio = 1:1). The cells were tested within a voltage window of 0.01–3 V (vs.  $\text{Li}/\text{Li}^+$ ) with Neware battery test system. The CV measurements were conducted at a scan rate of 0.1 mV s<sup>-1</sup> by using a CHI 600d electrochemical workstation. The EIS measurements were measured under frequency from 100 kHz to 0.1 Hz by utilizing a Parstat 2273 Advanced Electrochemical Systems apparatus. The OER performance was detected in 1.0 M KOH solution with a three-electrode system. The solution system should be aerated by flowing pure oxygen to make sure that the solution was oxygen-saturated. The slurry was fabricated by dissolving 5 mg of active material in 200 μL of 5 wt% Nafion solution which comprised deionized water, isopropanol and nafion at a volume ratio

of 4:1:0.05. The working electrode was prepared by dropwise adding 5  $\mu\text{L}$  of the as-fabricated slurry onto a glassy carbon electrode with 3 mm diameter (mass loading: 1.77  $\text{mg cm}^{-2}$ ). The Pt net and saturated calomel electrode (SCE) functioned as counter and reference electrodes, respectively. All potentials were converted to the reversible hydrogen electrode (RHE) based on the equation  $E (\text{vs. RHE}) = E (\text{vs. SCE}) + 0.244 + 0.059 \times \text{pH}$ . The linear sweep voltammetry (LSV) was conducted at a scan rate of 5  $\text{mV s}^{-1}$  within a voltage range of 0-0.8 V (vs. SCE). Before the LSV test, CV measurement was conducted at a scan rate of 10  $\text{mV s}^{-1}$  within the same voltage window until stabilization. The overpotential was calculated with the formula  $\eta = E (\text{vs. RHE}) - 1.23$ . The Tafel plots were fit to the Tafel equation ( $\eta = b \log(j/j^0)$ ), where  $\eta$  is the potential,  $b$  is the Tafel slope,  $j$  is the current density and  $j^0$  is the exchange current density.<sup>3</sup> EIS was performed under frequency from 100 kHz to 0.1 Hz. Chronoamperometry ( $I-t$ ) was tested at 1.57 V (vs. RHE) for 12 h. All the tests were carried out at room temperature (about 25°C).

**Characterizations:** XRD was conducted with a PANalytical X'pert PRO X-ray diffractometer with Cu K $\alpha$  radiation ( $\lambda = 0.154 \text{ nm}$ ). SEM was carried out by a Hitachi SU8000 microscope. BET measurements were tested by ASAP 2020. TEM and HRTEM were performed by a JEOL JEM-2100 microscope. Raman spectra were carried out using FT-Raman spectrometer (RFS 100/S, Bruker) with Nd: YAG laser at 1064 nm. XPS was performed by a Thermo Scientific K-Alpha spectrometer.

## Supplementary Figures and Tables

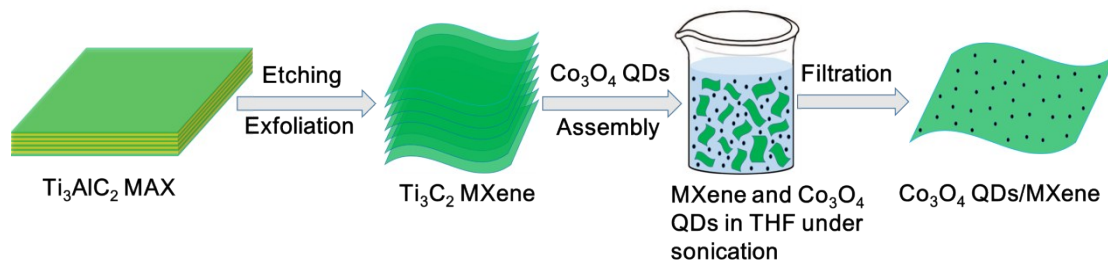


Fig. S1 The preparation of Co<sub>3</sub>O<sub>4</sub> QDs/MXene hybrids.

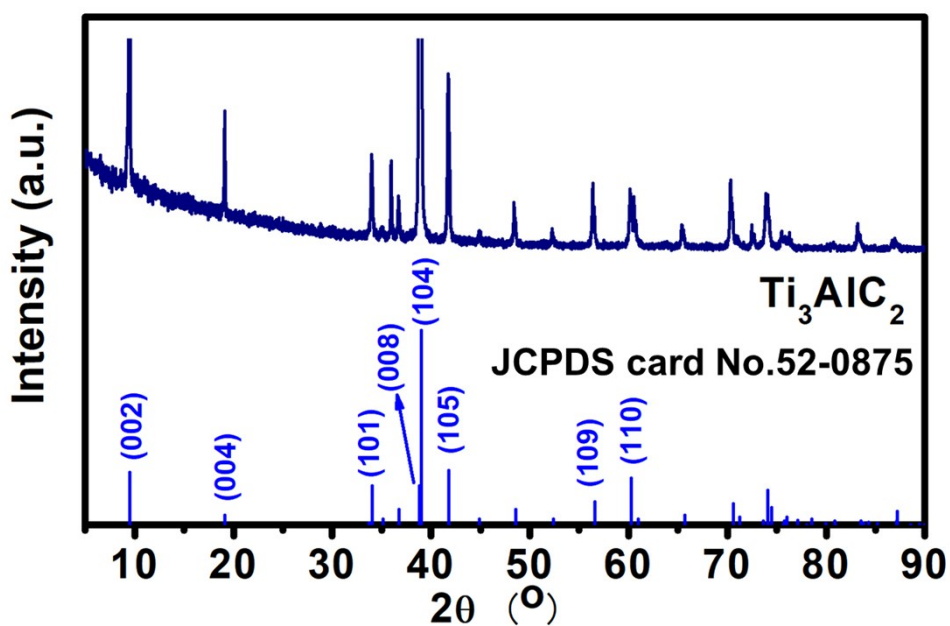


Fig. S2 XRD pattern of MAX phase and corresponding JCPDS card No. 52-0875.

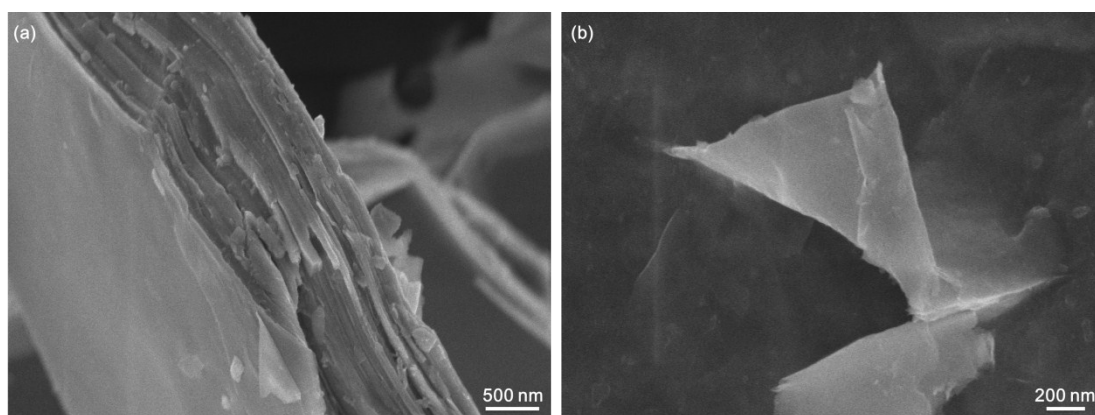
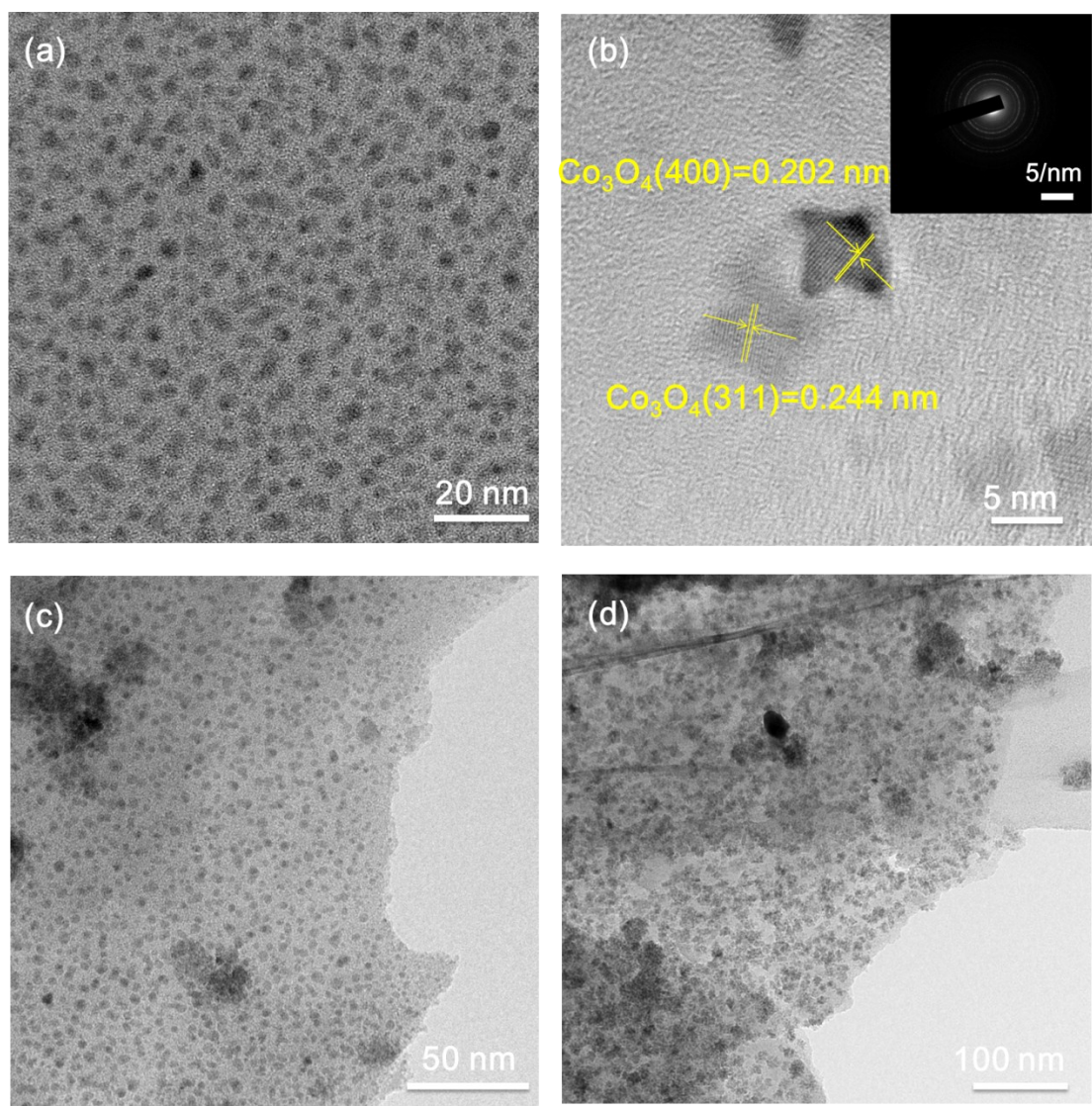


Fig. S3 SEM images of MAX (a) and MXene (b).



**Fig. S4 (a) TEM and (b) HRTEM images of  $\text{Co}_3\text{O}_4$  QDs with the SAED inset; TEM images of (c)  $\text{Co}_3\text{O}_4$  QDs/MXene-1:1 and (d)  $\text{Co}_3\text{O}_4$  QDs/MXene-3:1.**

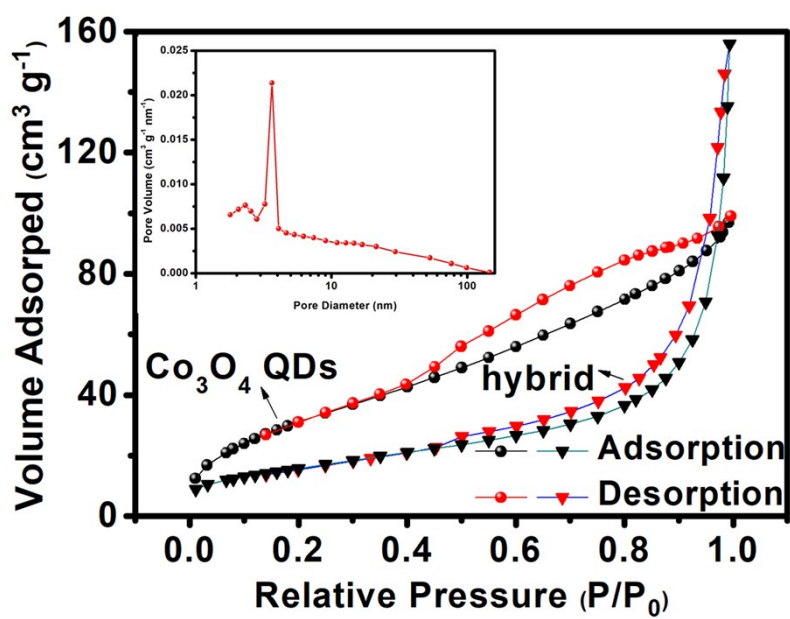
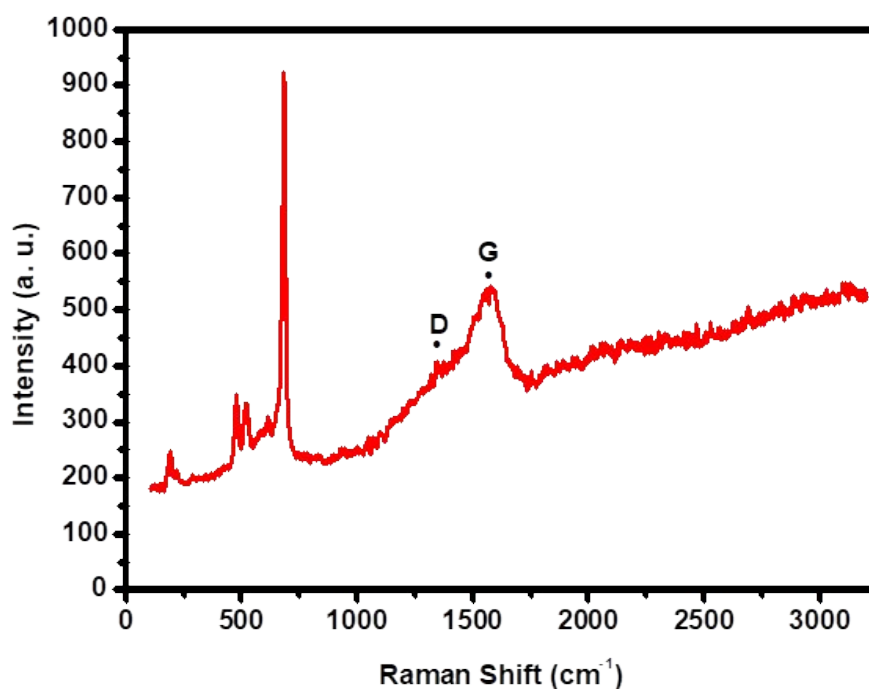


Fig. S5 Nitrogen adsorption-desorption isotherm of  $\text{Co}_3\text{O}_4$  QDs and  $\text{Co}_3\text{O}_4$  QDs/MXene hybrid-2:1. Inset: the corresponding pore size distribution of  $\text{Co}_3\text{O}_4$  QDs/MXene hybrid-2:1.



**Fig. S6 Raman spectrum of Co<sub>3</sub>O<sub>4</sub> QDs/MXene hybrid-2:1.**

The Raman spectrum of Co<sub>3</sub>O<sub>4</sub> QDs/MXene composite displayed in Fig.S5 exhibits five representative bands at ~ 192, 477 (E<sub>g</sub>), 520 (F<sub>2g</sub>), 615 (F<sub>2g</sub>) and 683 cm<sup>-1</sup> (A<sub>g</sub>), which are assigned to different vibrational modes of Co<sub>3</sub>O<sub>4</sub>.<sup>4</sup> The characteristic broad peak betwixt 1300 and 1600 cm<sup>-1</sup> can be ascribed to the carboneous materials, that is the minor peaks around 1346 (D band) and 1578 cm<sup>-1</sup> (G band) corresponding to disordered graphite from the defects in carbon materials and the vibration of sp<sup>2</sup> hybridized carbon atoms in 2D hexagonal lattice, respectively.<sup>5</sup> Above all, the Raman spectrum verifies the assembly of Co<sub>3</sub>O<sub>4</sub> QDs on 2D MXene nanosheets.

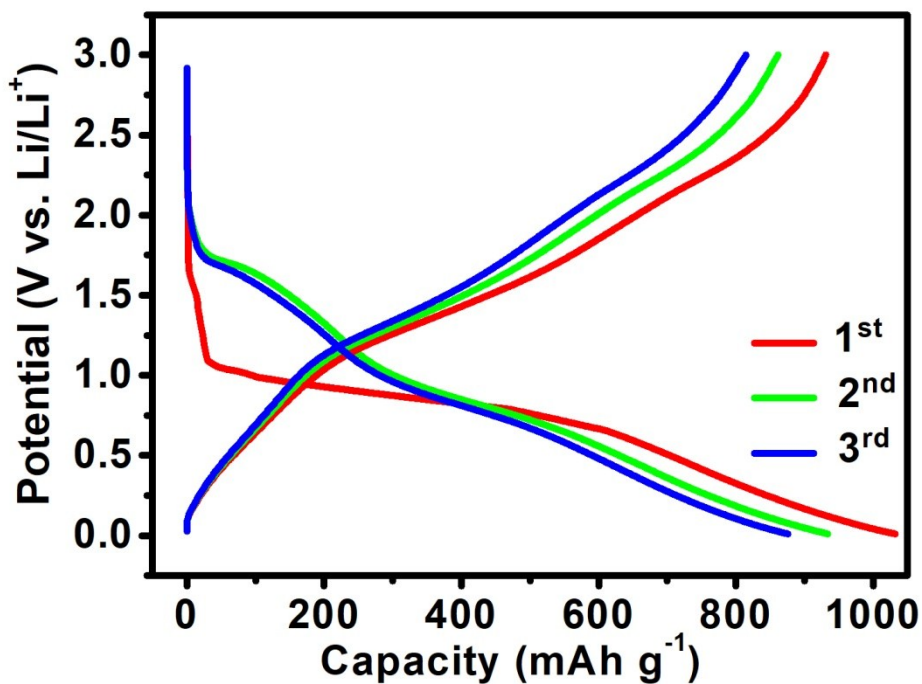


Fig. S7 Charge-discharge curves of  $\text{Co}_3\text{O}_4$  QDs/MXene hybrid-2:1 at  $100 \text{ mA g}^{-1}$ .

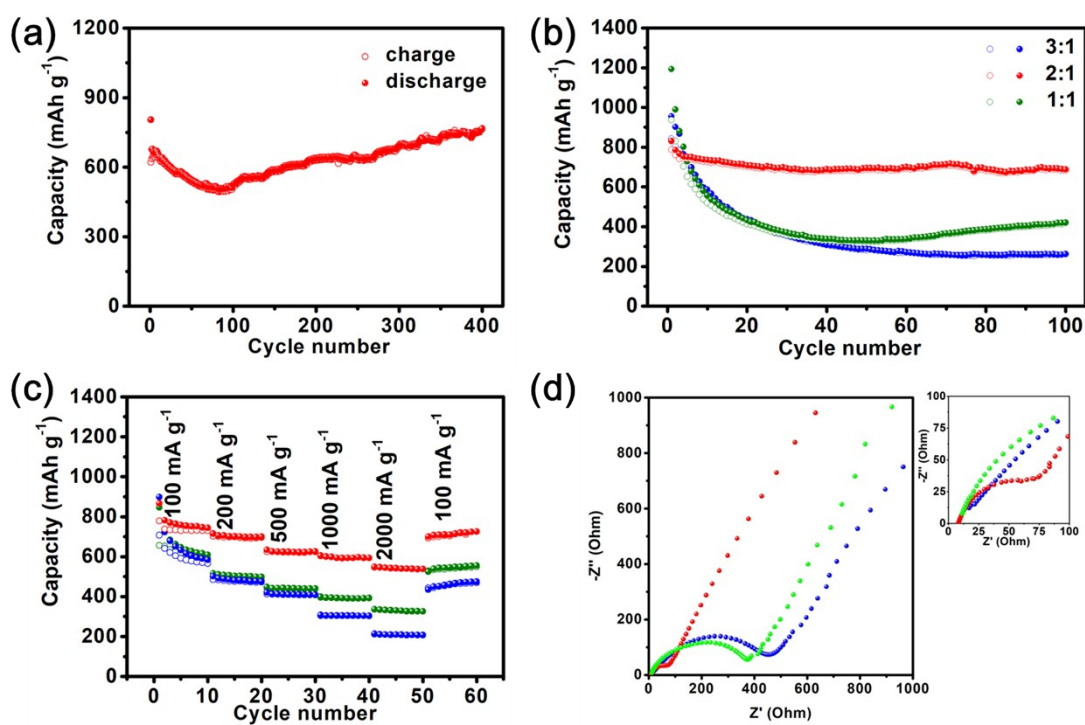


Fig. S8 Cycle properties of (a)  $\text{Co}_3\text{O}_4$  QDs/MXene hybrid-2:1 at  $2000 \text{ mA g}^{-1}$  and (b)  $\text{Co}_3\text{O}_4$  QDs/MXene hybrids at different mass ratios at  $200 \text{ mA g}^{-1}$ , (c) rate capabilities and (d) Nyquist plots of  $\text{Co}_3\text{O}_4$  QDs/MXene hybrids at different mass ratios.

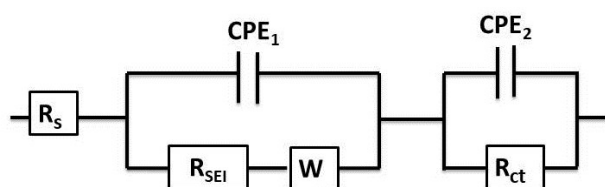


Fig. S9 Equivalent circuit for the EIS measurements.

**Table S1** The cycle and rate performances of our  $\text{Co}_3\text{O}_4$  QDs/MXene hybrid-2:1 and previously reported other  $\text{Co}_3\text{O}_4$ -based and MXene -based anodes.

Samples	Specific capacity ( $\text{mAh g}^{-1}$ )	High rate capacity	Reference
	(cycling numbers) (current density)	( $\text{mAh g}^{-1}$ )	
$\text{Co}_3\text{O}_4$ QDs/MXene	766.5 (400) (2.2C, 1C=890 $\text{mA g}^{-1}$ )	588.1 (2.2 C)	This work
$\text{Co}_3\text{O}_4/\text{C}$	490.5 (50) (0.5 C)	676 (2 C)	6
$\text{Co}_3\text{O}_4/\text{Graphene}$	631 (50) (0.06 C)	-	7
N, P-codoped C/ $\text{Co}_3\text{O}_4$	927 (100) (0.11 C)	454 (1.1 C)	8
MWCNTs/ $\text{Co}_3\text{O}_4$	813 (100) (0.11 C)	514 (1.1C)	9
$\text{Ti}_3\text{C}_2$ paper	410 (100) (0.36 C)	-	10
$\text{Ti}_3\text{C}_2/\text{CNTs}$	428 (300) (0.18 C)	218.2 (0.72 C)	11
PVP-Sn(IV)@ $\text{Ti}_3\text{C}_2$	544 (200) (0.63 C)	233 (3.37C)	12
$\text{SnO}_2@ \text{Ti}_3\text{C}_2$	360 (200) (0.11 C)	182 (0.11 C)	13

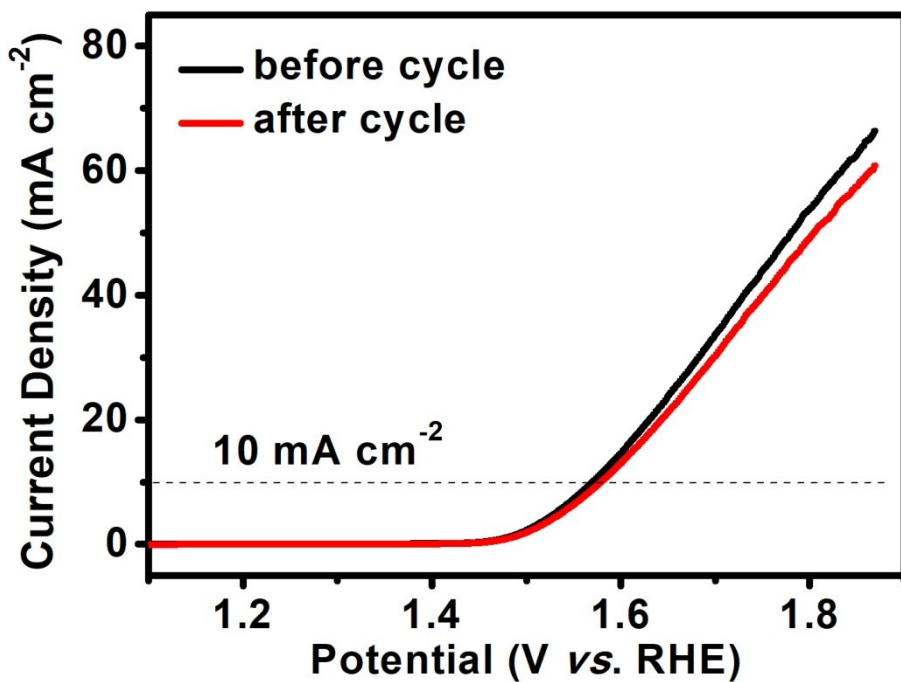


Fig. S10 LSV curves of  $\text{Co}_3\text{O}_4$  QDs/MXene hybrid-2:1 before and after 200 cycles.

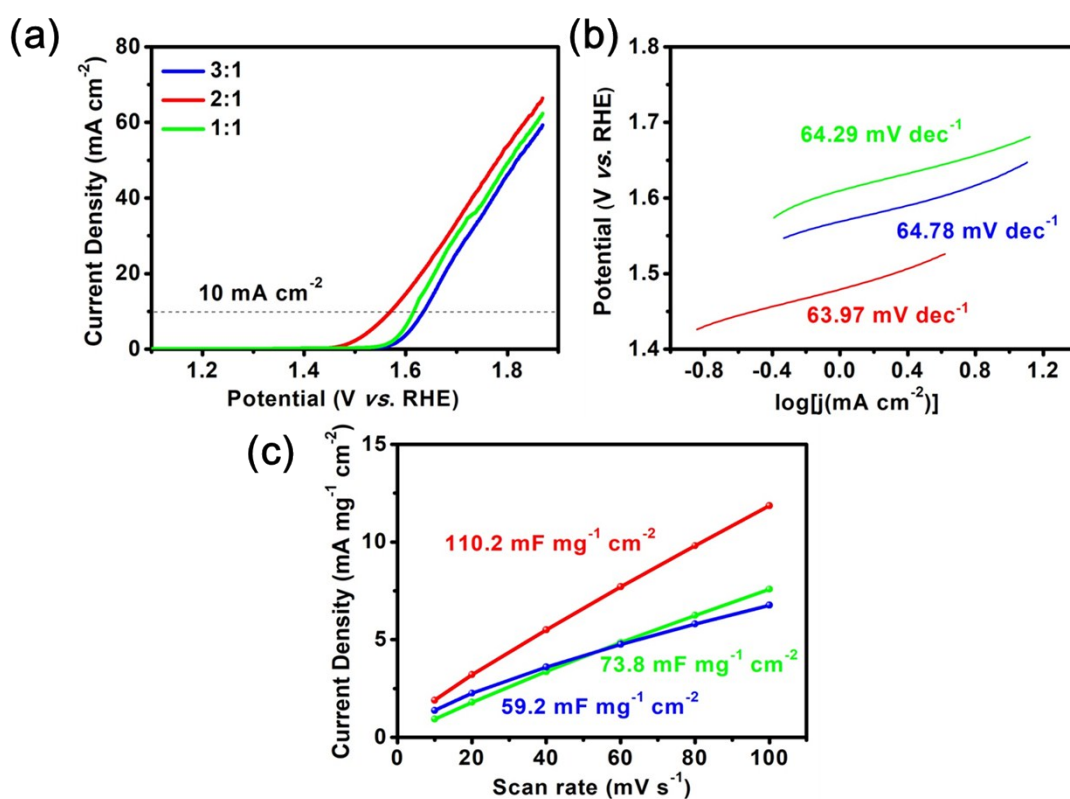


Fig. S11 (a) Polarization curves, (b) corresponding Tafel plots and (c) current density (at 1.22 V vs. RHE) vs. scan rate of the  $\text{Co}_3\text{O}_4$  QDs/MXene hybrids at different mass ratios.

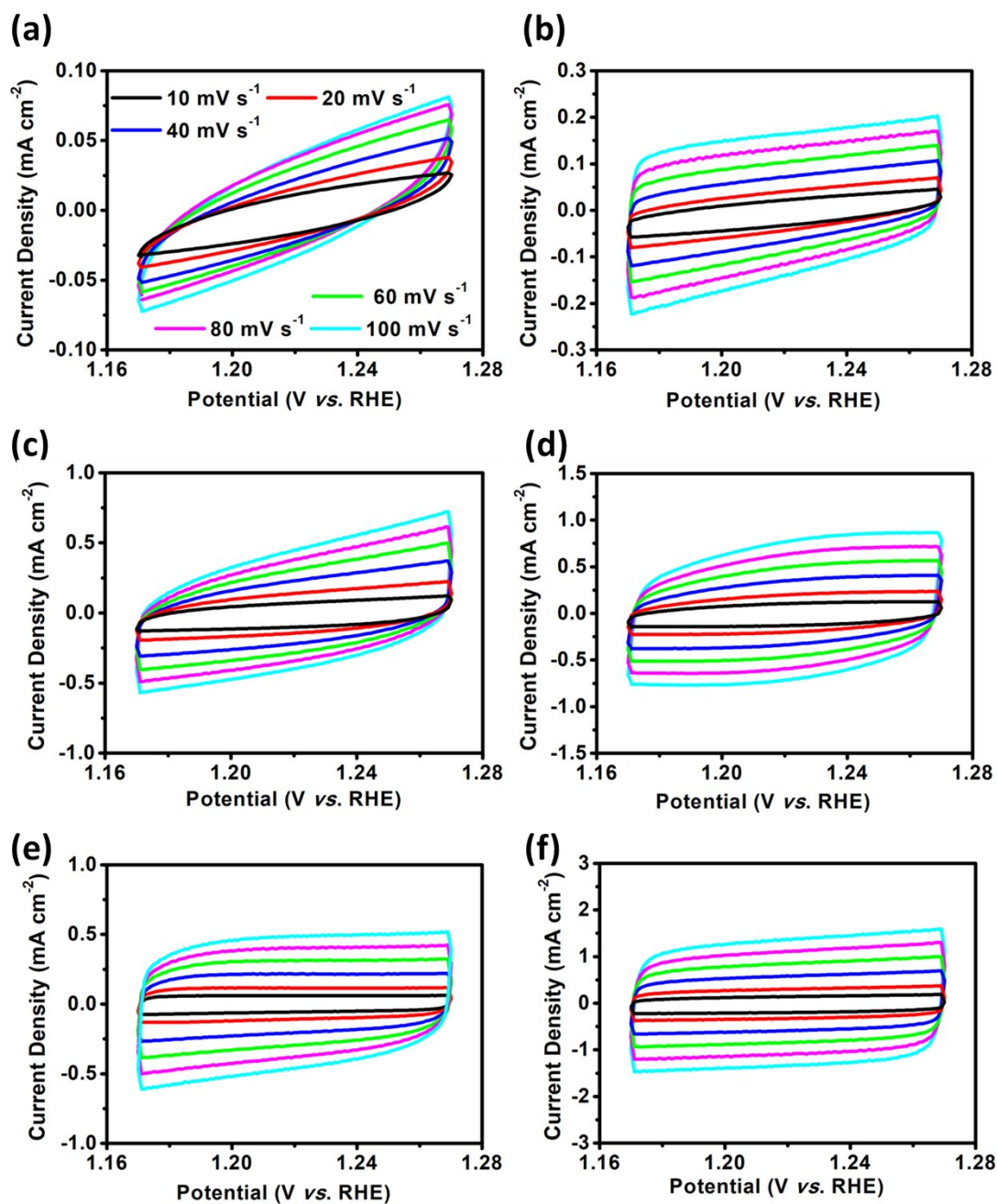


Fig. S12 EDLC curves of samples with different scan rates. (a) MXene nanosheets, (b) Co<sub>3</sub>O<sub>4</sub> QDs, (c) Co<sub>3</sub>O<sub>4</sub> QDs/MXene hybrid-1:1, (d) Co<sub>3</sub>O<sub>4</sub> QDs/MXene hybrid-2:1, (e) Co<sub>3</sub>O<sub>4</sub> QDs/MXene hybrid-3:1 and (f) RuO<sub>2</sub>.

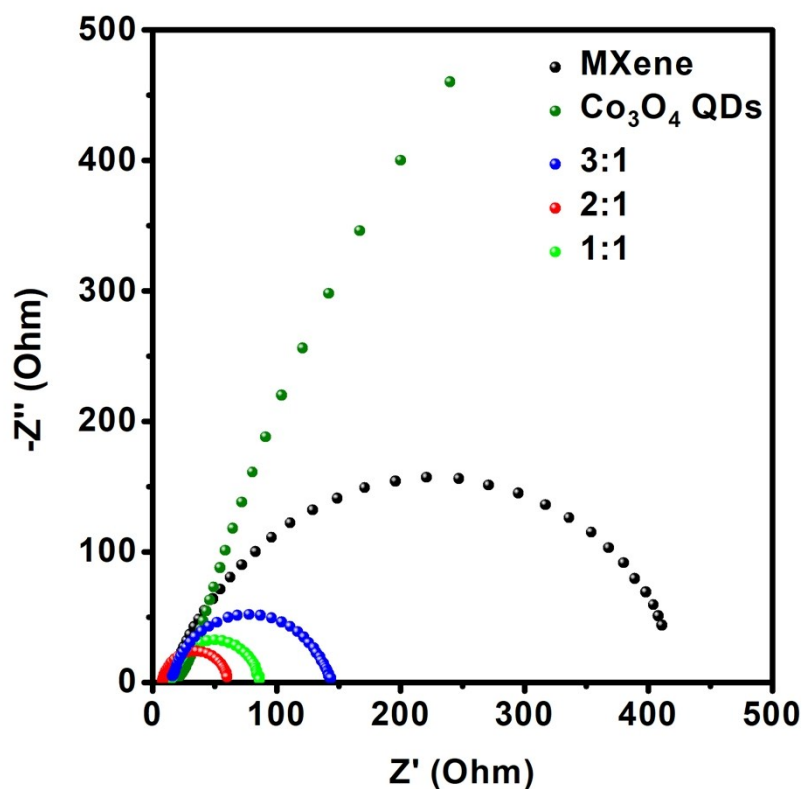


Fig. S13 Nyquist plots of MXene nanosheets,  $\text{Co}_3\text{O}_4$  QDs, and  $\text{Co}_3\text{O}_4$  QDs/MXene hybrids at different mass ratios.

Table S2 The OER performances of our  $\text{Co}_3\text{O}_4$  QDs/MXene hybrid-2:1 and previously reported, various  $\text{Co}_3\text{O}_4$ -based and MXene-based electrocatalysts.

Samples	Overpotential (mV) at $10 \text{ mA cm}^{-2}$	Tafel slope ( $\text{mV dec}^{-1}$ )	Testing environment	Reference
$\text{Co}_3\text{O}_4$ QDs/MXene	340	63.97	1.0 M KOH	This work
$\text{Co}_3\text{O}_4/\text{rGO}$	346	47	1.0 M KOH	14
Mesoporous $\text{Co}_3\text{O}_4$ nanoflakes	380	48	1.0 M KOH	15
$\text{Co}_3\text{O}_4$ nanooctahedras	530	-	0.1 M KOH	16
$\text{Co}_3\text{O}_4$ hollow polyhedrons	530	57	1.0 M KOH	17
$\text{C}_3\text{N}_4/\text{MXene-Ti}_3\text{C}_2$ film	420	74.6	0.1M KOH	18
$\text{Ti}_3\text{C}_2\text{T}_x\text{-CoBDC}$	410	48.2	0.1M KOH	19

## Supporting References

- 1 (a) S. Kajiyama, L. Szabova, K. Sodeyama, H. Linuma, R. Morita, K. Gotoh, Y. Tateyama, M. Okubo and A. Yamada, *ACS Nano*, 2016, **10**, 3334; (b) X. Xie, M. Q. Zhao, B. Anasori, K. Maleski, C. E. Ren, J. Li, B. W. Byles, E. Pomerantseva, G. Wang and Y. Gogotsi, *Nano Energy*, 2016, **26**, 513.
- 2 N. Shi, W. Cheng, H. Zhou, T. X. Fan and M. Niederberger, *Chem. Commun.*, 2015, **51**, 1338.
- 3 Schultze J. W. Sergio Trasatti (Ed.): *Electrodes of Conductive Metallic Oxides*, Part A. Elsevier Scientific Publishing Company, Amsterdam, New York, 1980.
- 4 J. Halim, M. R. Lukatskaya, K. M. Cook, J. Lu, C. R. Smith, L. Å. Näslund, S. J. May, L. Hultman, Y. Gogotsi, P. Eklund and M. W. Barsoum, *Chem. Mater.*, 2014, **26**, 2374.
- 5 (a) C. W. Tang, C. B. Wang and S. H. Chien, *Thermochim. Acta*, 2008, **473**, 68; (b) L. Y. Dong, C. G. Hu, X. K. Huang, N. Chen and L. T. Qu, *Chem. Asian J.*, 2015, **10**, 2609.
- 6 J. Chen, X. H. Xia, J. P. Tu, Q. Q. Xiong, Y. X. Yu, X. L. Wang and C. D. Gu, *J. Mater. Chem.*, 2012, **22**, 15056.
- 7 B. Wang, Y. Wang, J. Park, H. Ahn and G. Wang, *J. Alloy Compd.*, 2011, **509**, 7778.
- 8 Z. F. Wang, X. Zhang, Y. Sun, C. P. Wang, H. Zhang, Y. H. Shen and A. J. Xie, *J. Power Sources*, 2018, **740**, 446.
- 9 G. Huang, F. F. Zhang, X. C. Du, Y. L. Qin, D. M. Yin and L. M. Wang, *ACS Nano*, 2015, **2**, 1592.
- 10 O. Mashtalir, M. Naguib, V. N. Mochalin, Y. Dall'Agnese, M. Heon, M. W. Barsoum and Y. Gogotsi, *Nat. Commun.*, 2013, **4**, 1716.
- 11 Y. Liu, W. Wang, Y. Ying, Y. Wang and X. Peng, *Dalton Transactions*, 2015, **44**, 7123.
- 12 J. Luo, X. Tao, J. Zhang, Y. Xia, H. Huang, L. Zhang, Y. Gan, C. Liang and W. Zhang, *ACS Nano*, 2016, **10**, 2491.
- 13 F. Wang, Z. Wang, J. Zhu, H. Yang, X. Chen, L. Wang and C. Yang, *J. Mater. Sci.*, 2017, **52**, 3556.
- 14 M. Leng, X. L. Huang, W. Xiao, J. Ding, B. H. Liu, Y. H. Du and J. M. Xue, *Nano Energy*, 2017, **33**, 445.
- 15 S. Q. Chen, Y. F. Zhao, B. Sun, Z. M. Ao, X. Q. Xie, Y. Y. Wei and G. X. Wang, *ACS Appl. Mater. Interfaces*, 2015, **7**, 3306.
- 16 Z. Chen, C. X. Kronawitter and B. E. Koel, *Phys. Chem. Chem. Phys.*, 2015, **17**, 29387.
- 17 D. Dong, Y. Liu and J. Li, *Particle & Particle Systems Characterization*, 2016, **33**, 887.
- 18 T. Y. Ma, J. L. Cao, M. Jaroniec and S. Z. Qiao, *Angew. Chem. Int. Ed.*, 2016, **55**, 1138.
- 19 L. Zhao, B. L. Dong, S. Z. Li, L. J. Zhou, L. F. Lai, Z. W. Wang, S. L. Zhao, M. Han, K. Gao, M. Lu, X. J. Xie, B. Chen, Z. D. Liu, X. J. Wang, H. Zhang, H. Li, J. Q. Liu, H. Zhang, X. Huang, and W. Huang, *ACS Nano*, 2017, **11**, 5800.